processes

MDPI

Article

Catalytic Pyrolysis of Waste Plastics over Industrial Organic Solid-Waste-Derived Activated Carbon: Impacts of Activation Agents

Kezhen Qian [1,2,*], Wenmin Tian [1,2], Wentao Li [1,2], Shutong Wu [1,2], Dezhen Chen [1,2] and Yuheng Feng [1,2]

[1] School of Mechanical and Energy Engineering, Tongji University, Shanghai 200029, China
[2] Shanghai Engineering Research Center of Multi-Source Solid Waste Co-Processing and Energy Utilization, Shanghai 200092, China
* Correspondence: qiankz@tongji.edu.cn; Tel./Fax: +86-21-64251928

Abstract: Renewable source-derived carbon is found to be a green alternative catalyst to zeolite for the pyrolysis of plastics. However, only polyethylene (PE) catalytic pyrolysis over biomass-derived carbon has been extensively studied. In this work, carbon was produced from industrial organic solid waste using different activation agents, and their catalytic performance on the thermal degradation of typical polymers, namely PE, polypropylene (PP), polystyrene (PS), and polyethylene terephthalate (PET) were investigated. The degradation mechanisms and the roles of different active sites of the carbons are discussed. Steam failed to activate the carbon, which has a low specific surface area (6.7 m^2/g). Chemical activation using H_3PO_4 and $ZnCl_2$ produces carbons with higher specific surface area and more porosity. The pyrolysis characteristics of LDPE, PP, PS, and PET catalyzed by the carbons were studied using TGA and a fixed-bed reactor. The thermogravimetric results indicate that all three carbons reduce the pyrolysis temperature. The analysis of the products shows that the P- and Zn-involved acid sites on the AC-HP and AC-ZN change the reaction pathway of plastics and promote: (1) C-C cracking and aromatization of polyolefins; (2) the protonation of phenyl carbon of PS to yield higher benzene, toluene, and ethylbenzene; and (3) the decarboxylation of the terephthalic acid intermediate of PET, resulting in higher CO_2 and benzene. In addition, the high-value chemicals, long-chain alkylbenzenes, were found in the liquids of AC-ZN and AC-HP. The long-chain alkylbenzenes are probably formed by acid-catalyzed alkylation of aromatic hydrocarbons. This study provides basic data for the development of a cheap catalyst for plastic pyrolysis.

Keywords: industrial organic solid waste; carbon; pyrolysis of plastics; catalysis

Citation: Qian, K.; Tian, W.; Li, W.; Wu, S.; Chen, D.; Feng, Y. Catalytic Pyrolysis of Waste Plastics over Industrial Organic Solid-Waste-Derived Activated Carbon: Impacts of Activation Agents. *Processes* **2022**, *10*, 2668. https://doi.org/10.3390/pr10122668

Academic Editors: Zixu Yang and Kamil Witaszek

Received: 14 October 2022
Accepted: 5 December 2022
Published: 12 December 2022

1. Introduction

According to forecasts, the global commodity plastics market size is estimated to grow from USD 468 billion in 2020 to nearly USD 600 billion by 2025. Plastic waste generated in this manner is of serious concern since most of it ends up in landfills or is disposed of in the natural environment, endangering the environment [1,2]. Roughly 80% of the commodity plastics are polyethylene (PE), polystyrene (PS), and polyethylene terephthalate (PET) [3]. Incineration and mechanical recycling are not always feasible or sustainable for these plastics. Catalytic pyrolysis of plastics to produce valuable chemicals and fuels is a potentially appealing solution to eliminate plastic waste.

In China, industrial solid waste is a source of environmental contamination [4]. It is forecasted [5] that the amount of industrial solid waste in China will be 488 billion tons in 2025. However, only 50% of industrial solid waste was recycled [5]. A significant portion of the generated industrial solid waste was randomly disposed of or unreasonably treated [6]. Recently, more stringent control has been exercised on industrial solid waste management in China. A new ordinance stipulates that industrial solid waste disposal should be considered pollutant discharge and obey the pollution administrative permit

regulations. In such a scenario, the industrial solid waste treatment scale will increase significantly shortly.

The main components of industrial organic solid waste are carbon-rich materials, including paper, textiles, wood, plastics, rubber, etc. The current primary disposal and treatment methods for industrial organic solid waste are landfilling and co-incineration in municipal solid waste incinerating plants or coal-based power plants [7]. Moreover, valorizing organic waste into valuable chemicals and materials through a decentralized thermal conversion setup may be an alternative option.

Catalytic thermal conversion of carbon-rich feedstock into solid, liquid, and gaseous fuels over biomass-derived carbon catalysts has received considerable interest [8–10]. In recent years, carbon-biomass-based carbon was found to be a low-cost and sustainable catalyst for converting waste plastics [11,12]. Our previous works found that municipal solid-waste (MSW)-derived char can be used as a catalyst for tar reforming and syngas conversion [13,14]. The results showed that the MSW-derived char had better performance than the biomass (wheat straw)-derived char. Our studies indicated that MSW could also be a sustainable carbon source used to prepare carbon-based catalysts. In this context, since industrial organic solid waste has similar composition to municipal solid waste (MSW), we speculated that industrial organic solid waste could be a good precursor of carbon catalysts used to decompose plastics.

The carbons' performance is affected by the characteristics of the raw materials and the activating method. Tsyntsarski et al. [15] studied the catalytic performance of carbon prepared with different materials (peach stones, olive stones, and low-rank coal) for methanol decomposition. The structural parameters and acidic groups of carbon prepared from various raw materials differ. In addition, Fu et al. [16] found that high ash content may adversely affect the surface and pore structure development. Yeganeh et al. [17] also studied raw material's effect on the carbon's properties. They found that carbon from the hard shells of apricot stones had the best adsorption properties and the largest surface area. Industrial organic solid waste characteristics, such as organic structure and mineral composition, differ from biomass. The feasibility of applying industrial organic solid waste as carbon catalyst precursor should be evaluated.

The activating method changes the porosity, surface areas, and the surface functional groups, resulting in the variation of catalyst performance and even the degradation pathways. Sun et al. [12] investigated the catalytic reaction of mixed plastics (PE, PP, and PS) on biomass-derived carbon activated by three activators ($ZnCl_2$, H_3PO_4,, and KOH). The results indicated that the Lewis/Bronsted acid formed on the carbon facilitates the dehydrogenation process, hydrogen transfer reaction, Diels–Alder reaction, etc., promoting the conversion of olefins to aromatics. Zhang et al. studied the phosphoric acid activating condition on converting waste plastics into jet fuel [11]. They found the yield and composition of fuel can be regulated by adjusting the activating condition. However, the published studies only investigated the effect of activating conditions on the catalytic pyrolysis of plastic PE and mixed plastics over the biomass-derived carbon. Other major waste plastics, such as PP, PS and PET, were not studied.

This paper investigated the potential of applying industrial organic solid waste as a carbon catalyst precursor for the catalytic pyrolysis of waste plastics. The effects of activating method on the catalytic degradation pathways of different plastics (PE, PP, PS, and PET) were studied. The correlation between the active sites and the degradation mechanisms of various plastics was established.

2. Materials and Methods

2.1. Raw Materials

Industrial organic solid waste was collected from a municipal waste incineration plant in Zhejiang Province. The collected waste was dried, crushed, and sieved to a particle size of 0.4–0.8 cm. The industrial organic solid waste is composed of plastics, fabrics, paper, and wood. The plastics used in this study include low-density polyethylene (LDPE),

polypropylene (PP), polystyrene (PS), and polyethylene terephthalate (PET). Plastic samples were purchased from China Petroleum & Chemical Corporation. The composition and properties of solid waste are listed in Table 1.

Table 1. Characteristics of the industrial organic solid waste.

Property	Component	Concentration (wt.%)
Proximate analysis (wt.%, ad [a])	Moisture	1.26
	Ash	25.23
	Volatile	49.95
	Fixed-carbon	23.56
Ultimate analysis (wt.%, db [b])	C	42.51
	H	6.58
	N	0.55
	O [c]	50.36
Physical composition(wt %, ad [a])		
	Plastics	15
	Fabrics	20
	Paper	25
	Wood	40

[a] ad: Air-dry basis. [b] db: Dry basis. [c] O: Obtained by mass balance.

2.2. Sample Preparation

Steam, H_3PO_4, and $ZnCl_2$ were applied to prepare the carbon. The obtained carbons were abbreviated as c, AC-HP, and AC-ZN, respectively. It should be mentioned that name of AC-ST is just to be brief. The surface area of steam/carbon is low according to the BET test; thus, AC-ST should not be considered activated carbon.

The AC-ST was prepared via the pyrolysis/activation process. The industrial organic solid waste was pyrolyzed in nitrogen at 800 °C for 1.5 h and then activated at a steam flow rate of 7.6 g/min at 800 °C for 2 h. For AC-HP and AC-ZN, the waste was firstly soaked with a solution of H_3PO_4 or $ZnCl_2$ overnight. Then, the mixtures were dried and carbonized under an N_2 atmosphere at 500 °C for 2 h. The carbonized products were washed with distilled water until the pH reached neutral. The mass ratios of H_3PO_4 to industrial organic solid waste were 1:1, 1.5:1, and 2:1 (abbreviated as AC-HP1, AC-HP1.5, AC-HP2, respectively). The mass ratios of $ZnCl_2$ to industrial organic solid waste were 0.5:1, 1:1, and 1.5:1 (abbreviated as AC-ZN0.5, AC-ZN1, AC-ZN1.5, respectively).

2.3. Performance Test and Product Analysis

The catalytic pyrolysis of plastics was carried out on a two-staged fixed-bed reactor (Figure 1). The plastic and carbon were filled in the upper and bottom stages. The quartz wool was used to support the plastic and catalyst. Before the reaction, the reactor was purged with 100 L/min nitrogen for 10 min. When the bottom stage was kept at a constant temperature of 500 °C, the upper stage was heated to 500 °C at a heating rate of 10 °C/min with a dwell time of 20 min. The liquid products were collected in two condensing bottles cooled with dry ice. The gas products were sampled with gas bags. After the reaction, the condensing bottles, quartz tubes, and connecting tubes were weighed to calculate the oil and solid residue mass. The gas yield was calculated by mass balance.

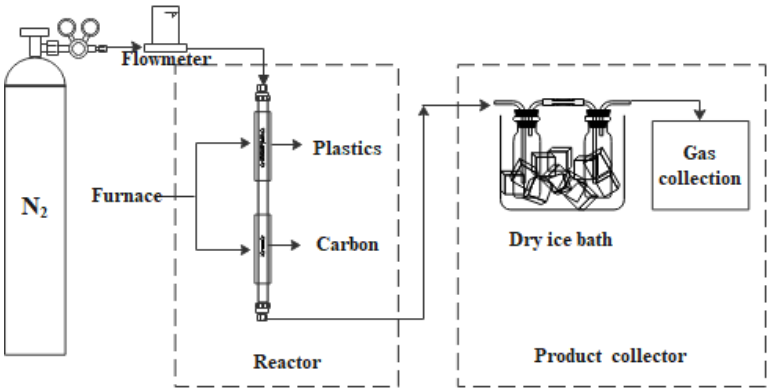

Figure 1. Catalytic pyrolysis setup.

The liquid products were analyzed by gas chromatography-mass spectrometry (GCMS-QP2010, Shimadzu, Japan) equipped with an RTx-5 column. The gas products were (CO, CO_2, H_2, O_2, CH_4, C_2H_4, C_3H_6, C_4H_8, etc.) analyzed by a gas chromatograph equipped with a TCD and an FID (7820 A, Agilent, Santa Clara, CA, USA)

The thermogravimetric analyzer studied the pyrolysis characteristics of plastics mixed with carbon. The samples of approximately 10 mg carbon and 10 mg plastics were heated from room temperature to 800 °C at a heating rate of 10 °C/min under 100 mL/min N_2.

The adsorption/desorption isotherms were measured on the Micromeritics ASAP 2420 instrument. All samples were degassed at 573 K for 6 h. The specific surface area was calculated according to the Brunauer–Emmett–Teller (BET) theory. The information on the micropore and mesopore was obtained by the HK and BJH methods. Identifying surface functional groups on carbon was carried out using a Fourier transform infrared spectroscopy (FTIR). Graphite properties of the samples were evaluated by Raman spectroscopy.

We also calculated the activation energy. The plastic pyrolysis reaction follows the non-isothermal and heterogeneous reactions [18]. The kinetics of pyrolysis is usually described by Equation (1):

$$\frac{d\alpha}{dt} = kf(\alpha) = A\exp(-\frac{E}{RT})f(\alpha) \quad (1)$$

where t is the pyrolysis time (min), $d\alpha/dt$ is the rate of conversion during pyrolysis, f (α) is the differential reaction model to be decided by the reaction. E, A, and R are the activation energy (KJ/molK), pre-exponential constant, and the universal gas constant (8.314 J/molK), respectively. T is the absolute temperature (K).

α is the extent of the reaction (%) during the thermal degradation. α can be defined as the ratio of weight loss at time t to the total weight loss corresponding to the degradation process, $\alpha = \frac{M_0 - M_t}{M_0 - M_f}$, where M_0 is the initial mass of the sample, and M_t and M_f are the mass at time t and the final mass of the sample, respectively.

The heating rate during the experiment is β = dT / dt = const, combining β into Equation (1) as:

$$\frac{d\alpha}{dT} = (\frac{A}{\beta})\exp(-\frac{E}{RT})f(\alpha) \quad (2)$$

Integrating both sides of Equation (2) by the Coats–Redfern method, multiplied by $1/T^2$, and taken by the natural logarithm:

$$\ln[\frac{G(\alpha)}{T^2}] = \ln\frac{AR}{\beta E} - \frac{E}{RT} \quad (3)$$

$y = \ln[\frac{G(\alpha)}{T^2}]$ and $x = 1/T$ are linearly fitted, and E can be calculated from the slope. $G(\alpha)$ is the integral reaction model function to be determined for a particular pyrolysis process. The pyrolysis intervals in Table S1 were used to calculate the activation energy of the reaction.

3. Results and Discussion

3.1. BET, FTIR, and Raman Spectroscopy

Table 2 shows that AC-HP and AC-ZN have a specific surface area of 606.08 m^2/g and 752.95 m^2/g and an average pore size of 2.34 nm and 2.67 nm, respectively. Contrarily, the specific surface area of carbon prepared by steam activation is only 6.68 m^2/g, and the total pore volume is about 0.018 cm^3/g, suggesting that the steam activating condition may not effectively activate the industrial organic solid-waste-derived carbon. The AC-HP and AC-ZN show the typical IV isotherm and H4 hysteresis curves, indicating they are mesoporous materials. Figure S1b shows that the carbon contains micropores and mesopores [19].

Table 2. Mass yields of the obtained carbon materials and their surface areas and pore properties.

Sample	Yield (wt.%)	S_{BET} (m^2/g) [a]	S_{Micro} (m^2/g) [b]	S_{Ext} (m^2/g) [c]	V_{Total} (cm^3/g) [d]	V_{Meso} (cm^3/g) [b]	$D_{Average}$ (nm) [e]
AC-ST	18.72	6.68	1.77	4.91	0.02	0.01	11.70
AC-HP	45.74	606.08	286.28	319.80	0.34	0.18	2.34
AC-ZN	48.04	752.95	458.41	294.54	0.46	0.15	2.67

[a] Calculated by multipoint BET method. [b] Determined by t-plot method. [c] By difference. [d] Calculated from absorbed volume of nitrogen for a relative pressure P/P_0 of 0.99. [e] Determined by BJH method.

The FTIR spectra of AC-HP and AC-ZN are shown in Figure 2, which identify the functional groups on the carbons. All the samples contain peaks at 1164 cm^{-1}, 1690–1594 cm^{-1}, and 3500 cm^{-1}. The peak at 1164 cm^{-1} is related to C-O vibrations, whereas the peak at 1690–1594 cm^{-1} is related to C=O stretching vibrations [20]. The peak at 3500 cm^{-1} corresponds to the −OH stretching, which might be related to the adsorbed water, carboxyl groups, or −OH vibrations of the phosphate group in AC-HP [21,22]. The slight shoulder at 1265 cm^{-1} implies the presence of P=O groups on carbon [23,24].

The Raman spectrum (Figure 2) has two peaks near 1598 cm^{-1} and 1350 cm^{-1}, referred to as the G (graphite or ordered) and D (disordered) bands, respectively [25]. The intensity ratio of the two peaks was determined using Gaussian fitting. The I_D/I_G for AC-HP and AC-ZN are 0.94 and 0.97, respectively, indicating AC-HP and AC-ZN have a similar degree of graphitization. The degree of graphitization of the used AC-HP and AC-ZN did not change significantly, and their I_D/I_G values are 0.98 and 1.05, respectively.

3.2. Pyrolysis Behaviors of Plastics and Carbon Mixture

Figure 3 shows TG and DTG curves of catalytic pyrolysis of plastics over carbons. The carbon was evenly mixed with the plastics. Temperatures from weight loss above 0.02 wt./°C% to weightlessness are considered pyrolysis intervals. The temperature at the maximum weightlessness rate is denoted as T_{peak}. Table S1 lists the pyrolysis intervals and T_{peak}.

The AC-ST, AC-HP, and AC-ZN were thermally stable before 500 °C. All four raw plastics did not lose weight when the pyrolysis temperature was below 350 °C. The PS has the lowest pyrolysis interval (348–460 °C) and T_{peak}, while the LDPE has the highest interval (398–500 °C) and T_{peak}. These data were consistent with the findings that the thermal stability order of different plastics was LDPE > PP > PS [26].

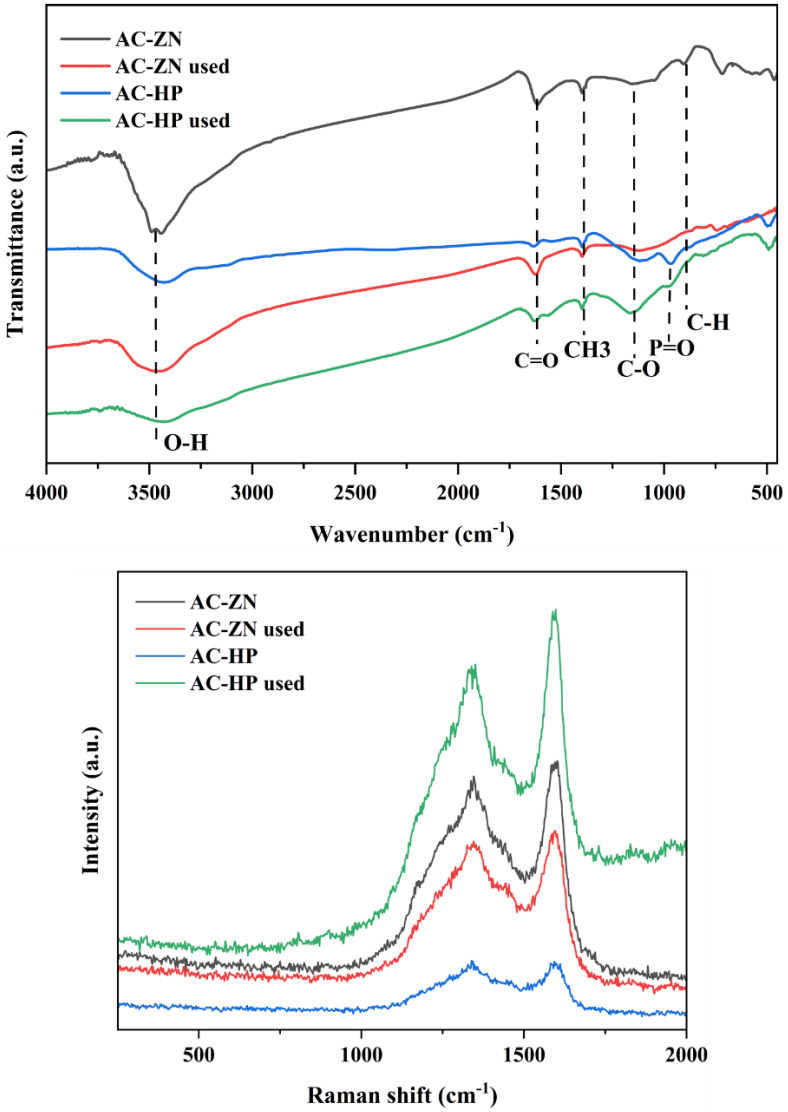

Figure 2. FT-IR spectra and Raman spectra of AC-ZN and AC-HP.

When the plastics were catalytically pyrolyzed with AC-ST, AC-HP, and AC-ZN (Figure 3), the initial degradation temperatures and T_{peak} of LDPE, PP, and PS were reduced by 20–50 °C and 20–30 °C, respectively, indicating that the carbons decrease the thermal stability of LDPE, PP, and PS. However, for PET, the carbons did not significantly change their initial degradation temperatures and T_{peak}. The reduction effect of AC-ST, AC-HP, and AC-ZN differs with different plastics. No significant difference was found in the decrease in initial degradation temperature and T_{peak} for LDPE over three carbons. Contrarily, the AC-HP and AC-ZN have a noteworthy effect on initial degradation temperature and T_{peak} on PP and PS.

The activation energies are shown in Table S1. AC-ST, AC-HP, and AC-ZN all reduce the activation energy of plastic pyrolysis. The order of reducing effect on the pyrolysis activation energy of plastics is AC-ST < AC-HP < AC-ZN.

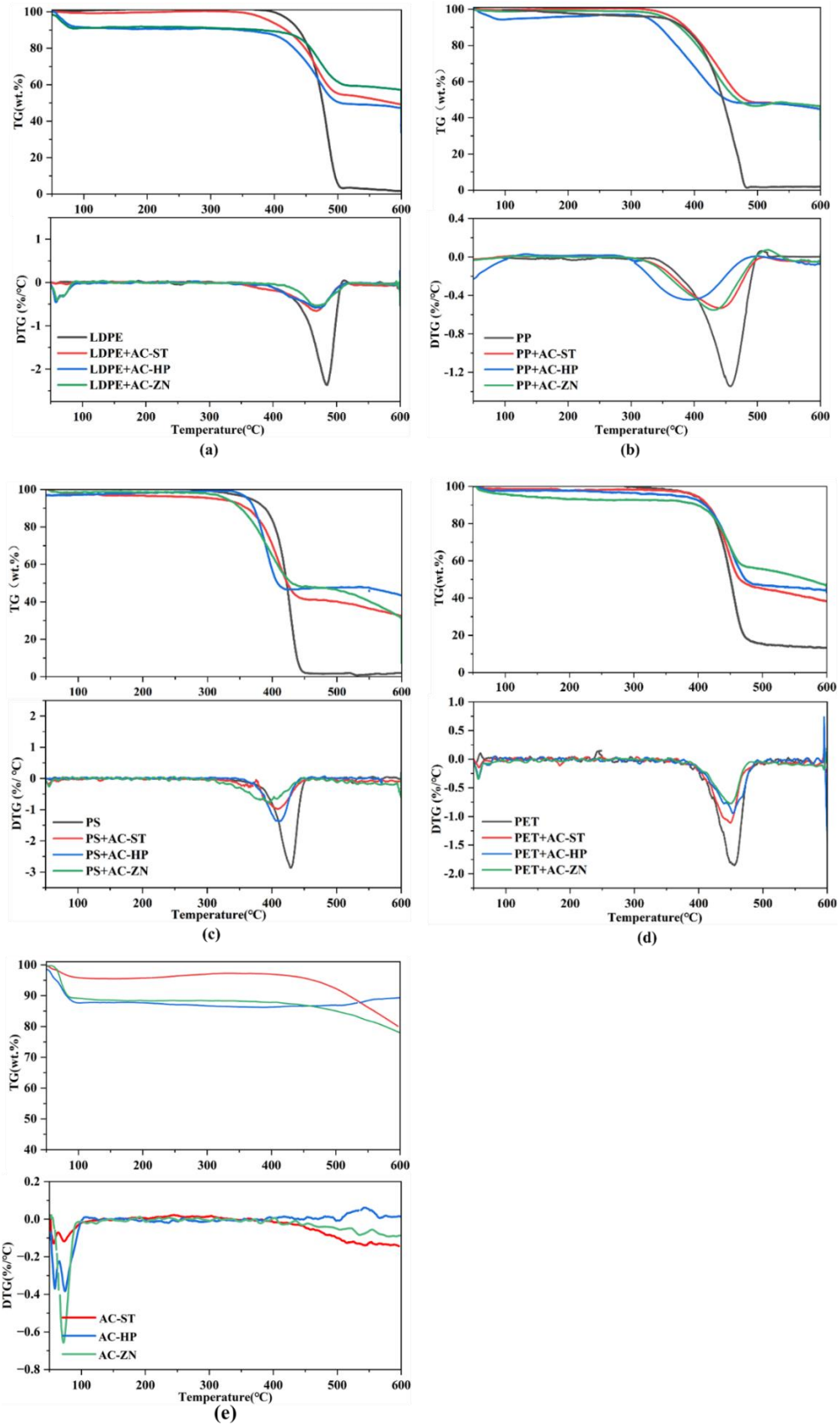

Figure 3. The TG and DTG curves of (**a**) LDPE, (**b**) PP, (**c**) PS, (**d**) PET, and (**e**) carbon catalyst thermal pyrolysis and catalytic pyrolysis with carbons. Conditions: heating rate = 10 °C/min; N_2 atmosphere; carbon 10 mg and plastic 10 mg.

3.3. Catalytic Performance of Carbon on Pyrolysis of Plastic

3.3.1. Product Yields

Figure 4 shows the yields of products of catalytic pyrolysis of LDPE, PP, PS, and PET. We also conducted thermal pyrolysis of LDPE, PP, PS, and PET without carbon, and the products are mainly solid-phase wax at room temperature with limited gas production. Under the catalytic condition, all three carbons enhance the depolymerization of LDPE, PP, and PS but with different effects. For LDPE, the AC-ST, AC-HP and AC-ZN increased the yields of gaseous products to 28.59, 63.84, and 66.00 wt.% and the yields of liquids to 10–60% wt.%. The catalytic pyrolysis of PP and PS yields mainly liquid (53.66–67.74 wt.% and 67.2–88.16 wt.%, respectively).

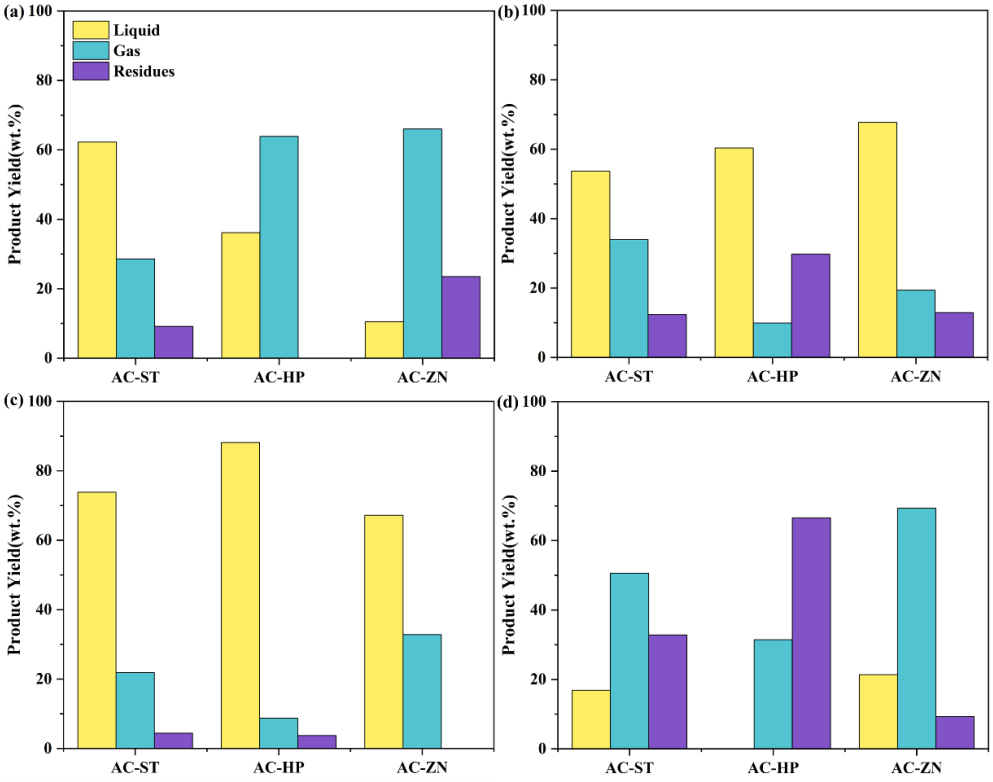

Figure 4. Product yields of (**a**) LDPE, (**b**) PP, (**c**) PS, (**d**) PET under different carbons.

The carbons enhance the decomposition of PET to a lesser extent than LDPE, PP, and PS, as PET has higher thermal stability [27]. AC-ST and AC-ZN produce 50 and 70 wt.% gas, mainly derived from the decarboxylation of constituent monomers [28]. Under the catalysis of AC-HP, the catalytic pyrolysis of polyethylene terephthalate (PET) produces about 66 wt.% solid residues indicating the AC-HP is not highly effective in enhancing the decomposition of PET.

3.3.2. Product Compositions

Figures S2 and S3 show the carbon number distribution of the products produced by the catalytic cracking of LDPE and PP over AC-ST, AC-HP, and AC-ZN. The product obtained without carbon contains components that cannot be identified and analyzed by the herein applied GC-MS methods. The carbon number of liquid LDPE catalytic pyrolysis products is mostly less than 25. The average carbon number of liquid of LDPE follows the order of AC-ZN < AC-HP < AC-ST. The lower average number of AC-ZN and AC-HP indicates that the AC-ZN and AC-HP have a higher catalytic effect on promoting the scission of the LDPE backbone. This is because Zn and P in the carbon create active acid sites for forming carbonium ions or carbenium ions. The lower average carbon number of AC-ZN than that of AC-HP was probably due to two reasons. Firstly, the Zn-correlated

Lewis acid may cooperate with the Bronsted acid to enhance the activation of the C-C bond. Secondly, AC-ZN has a higher surface area and thus has more accessible active sites than AC-HP.

Table 3 shows the compositions of the liquid products produced by LDPE and PP catalytic cracking. LDPE's liquid composition mainly includes alkanes, olefins, and aromatics and varies with carbons. Under the catalysis of AC-ST, straight alkanes and straight olefins in the diesel range (C8-21) are the primary compounds in liquid, with a fraction of 58.8% and 31.89%, respectively. No aromatics were found in the product of LDPE under the catalysis of AC-ST. The alkanes in the liquid present a random distribution spectrum, indicating that the random chain-breaking [29] occurred.

Table 3. The composition of liquid obtained by the cracking of LDPE and PP.

Product	LDPE (area%)			PP (area%)		
	AC-ST	AC-HP	AC-ZN	AC-ST	AC-HP	AC-ZN
Alkanes	57.34	60.21	48.56	17.88	24.65	14.11
Straight Alkanes	57.34	60.21	48.56			
Branched Alkanes				4.93	2.08	11.9
Cycloalkanes				12.95	22.57	2.21
Alkenes	36.82	13.68		67.44	29.56	43.84
Straight Alkenes	36.82	0.42		4.44	2.1	
Branched Alkenes		13.26		61.71	1.24	41.75
Cycloalkenes				1.29	26.22	2.09
Aromatics		22.02	49.77	0.71	37.06	41.47
Benzene						0.57
Toluene		0.36	0.66			5.16
Ethylbenzene		0.34	1.12			0.58
Xylene		0.61	2.11		2.04	11.71
Mesitylene		0.16	0.5	0.71	19.01	15.76
Chain alkyl Aromatics		10.61	25.62		14.11	6.6
Naphthalenes		7.73	11.09		1.9	1.09
Other PAHs		2.21	8.67			
Others	3.62	3.7	1.67	13.97	8.73	

The acid sites on AC-HP and AC-ZN promote the conversion of olefins intermediates to aromatics. When AC-HP is used as a catalyst, the olefins reduce to 13.68%, and the aromatics increase to 22.02%. In addition, data show that the AC-HP yields relatively higher alkanes in gas, indicating that hydrogen transfer occurs during aromatic formation on AC-HP. The published studies regarding the conversion of polyethylene to aromatics over carbon have no solid evidence to give conclusive results of the reaction mechanism. It is usually believed that the transformation of alkanes or olefins to aromatic over solid acids is through the cyclization of two olefins or diolefins with the companion of hydrogen transfer or direct dehydrogenation [30,31], depending on the nature of the acid. The Bronsted acid, such as COOH, on AC-HP catalyzes cyclization of olefins and hydrogen transferring to form aromatics. The Lewis acid groups, such as P=O and C=O, may catalyze dehydrogenation. Meanwhile, the cooperation of P=O and C=O may also occur—P=O can act as an electron donor to enhance the C=O active site's dehydrogenation activity [32]. When the AC-ZN catalyzes the LDPE pyrolysis, the olefin fraction further reduces to zero, and aromatics increase to about 53%. The high aromatics yield over AC-ZN relates to its presence of the Zn-involved acid sites. The publications show that the aromatization of olefins over Zn-involved acid sites occurs mainly through cyclization of diolefins followed by direct dehydrogenation. This reaction mechanism requires lower energy than that over the Bronsted acid site, yielding higher aromatics.

Interestingly, we also found the long-chain alkylbenzenes, a high-value chemical, in the liquids of AC-ZN and AC-HP. The long-chain alkylbenzenes are probably formed by acid-catalyzed alkylation of aromatic hydrocarbons [12].

Table 4, Figures S4 and S5 show the composition carbon distribution of the products produced by catalytic cracking of PS and PET over AC-ST, AC-HP, and AC-ZN. The primary component in the liquid of PP catalyzed by AC-ST is branched olefins derived from mid-chain scission and intramolecular hydrogen transfers of the PP carbon chain (P6 and 7, Scheme 1b) [33]. Compared to AC-ST, the AC-HP liquid products have a lower fraction of branched olefins and a higher fraction of cycloolefins, cycloalkanes, and aromatics. This is because the Bronsted acid promotes the cyclization of olefins. The major compounds in the liquid of AC-ZN are branched olefins and aromatics. The AC-ZN produces fewer cycloolefins and cycloalkanes than AC-HP because AC-ZN has fewer Bronsted acid sites for cyclization. In addition, the AC-ZN produces benzene, toluene, and ethylbenzene, which are not found in the liquid of AC-ST and AC-HP. The benzene, toluene, and ethylbenzene are most likely generated by the dehydrogenation of cycloalkanes and cycloalkene over Zn species [34]. We also found a considerable amount of mesitylene (19.01% and 15.76%) in the PP pyrolysis liquid of AC-HP and AC-ZN. The mesitylene is probably generated via cyclization and dehydrogenation (P4, Scheme 1b) of trimethyl alkane and olefins that significantly exist in the liquid product of PP pyrolysis.

As shown in Table 4, the catalytic pyrolysis of PS over AC-ST, AC-HP, and AC-ZN primarily produce PS's monomer styrene, indicating that the end-chain-scission is the principal reaction during PS degradation [35]. Additionally, benzene, toluene, ethylbenzene, and α-methyl styrene were also produced. Benzene and toluene may be formed through protonation of the carbon on the aromatic ring [36], which then undergoes β-scission to form benzene and toluene, respectively. The α-methyl styrene is probably generated via the activation of carbon on the aliphatic chain by Bronsted acid, followed by β-scission and hydrogen rearrangement [37].

Compared with AC-ZN, the ethylbenzene content significantly increases when AC-HP and AC-ZN are used as catalysts. The ethylbenzene can be produced through β-Scission of carbocations (P6, Scheme 1c) or hydride transfer of a triple-coordinated carbocation (P4, P5, Scheme 1c) [38]. However, which acid site played the critical role is not reported in the literature. Researchers studied the catalytic degradation of PS over the Bronsted-acid-dominated catalyst (HZSM-5 and HY) with the highest fraction of 16.2% for ethylbenzene [39,40]. In contrast, in our experiments, ethylbenzene reaches as high as 28.59%. This indicates that the P- and Zn-involved Lewis acid sites on the carbon played an important role.

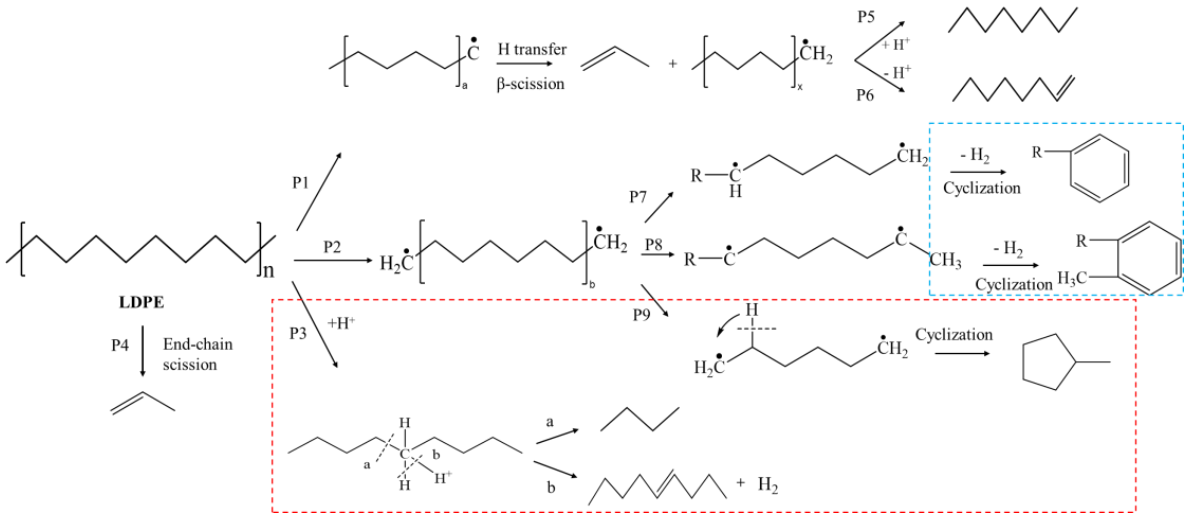

(**a**)

Scheme 1. *Cont.*

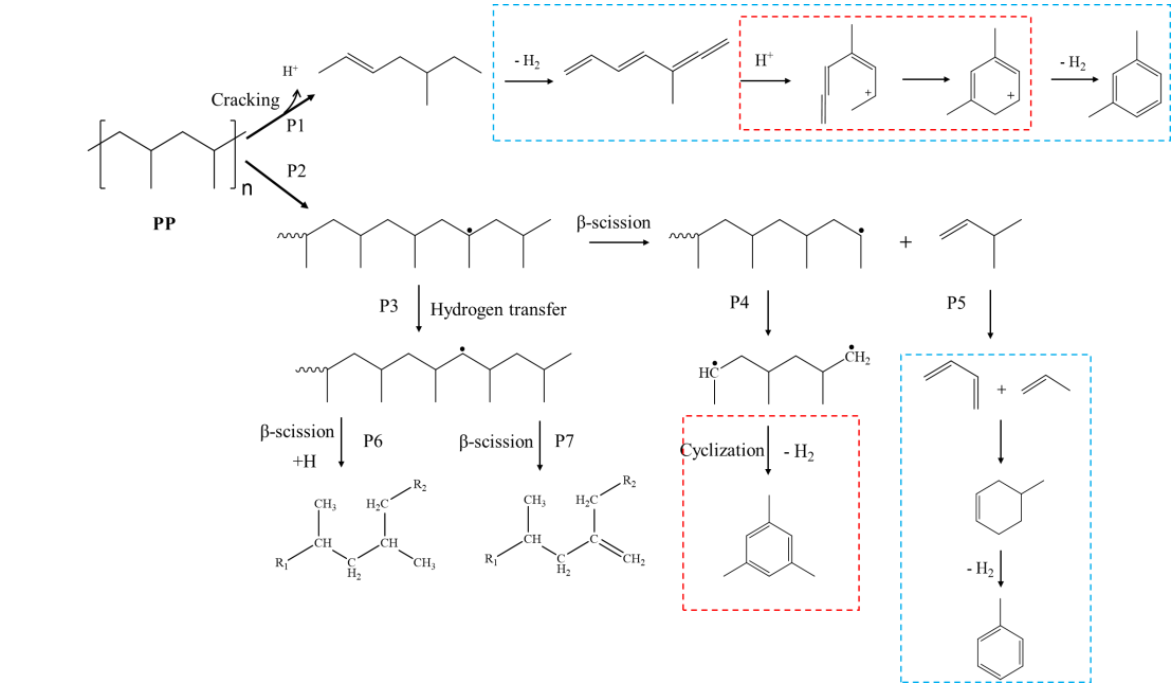

(**b**)

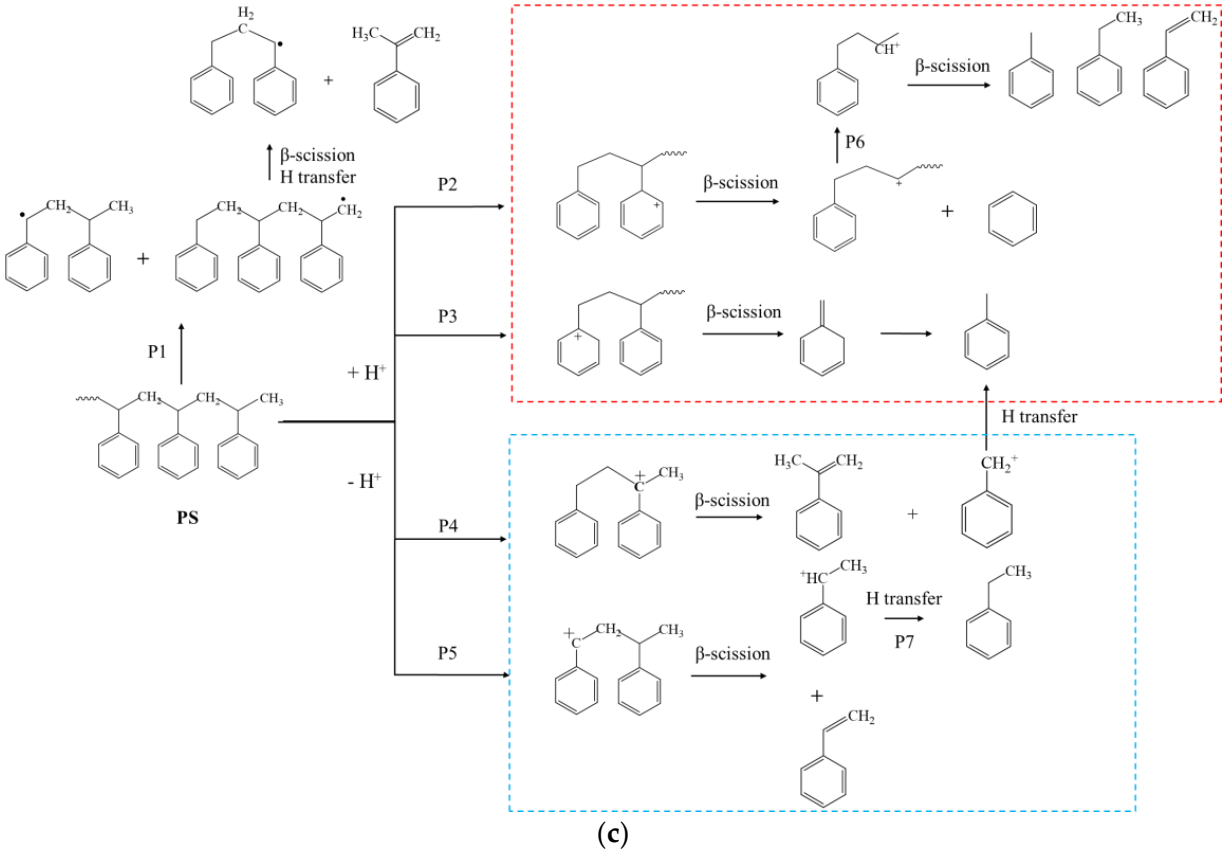

(**c**)

Scheme 1. *Cont.*

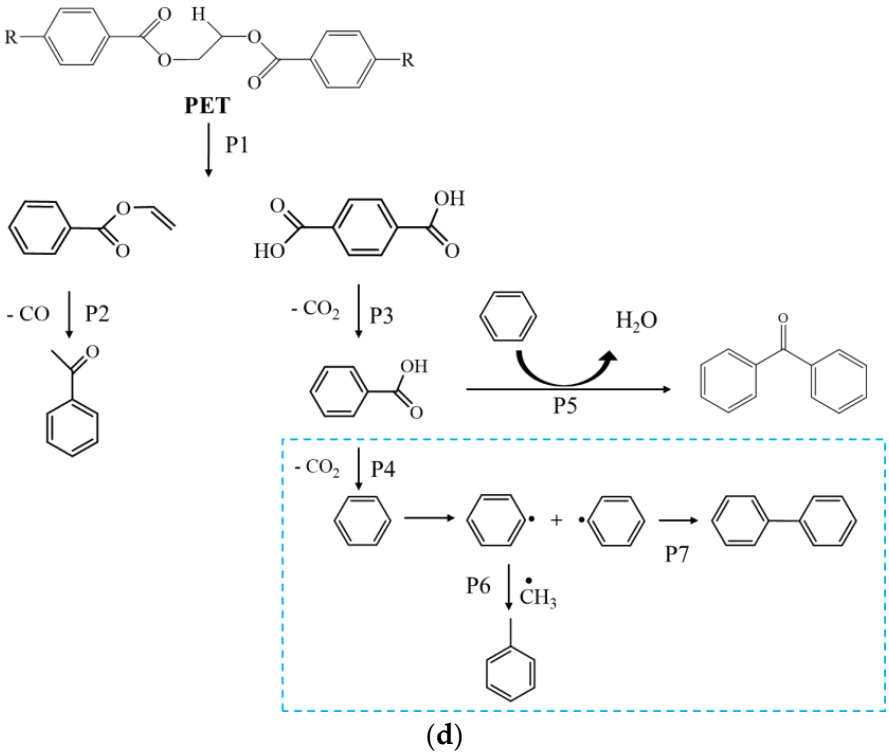

Scheme 1. Possible reaction pathways for (**a**) LDPE, (**b**) PP, (**c**) PS, and (**d**) PET catalytic pyrolysis. The red frame represents the reactions promoted Bronsted acid on carbon. The blue frame represents the reactions promoted by Zn- or P-involved species.

Table 4. The composition of liquid obtained by the cracking of PS and PET.

Product	PS (area%)			PET (area%)	
	AC-ST	AC-HP	AC-ZN	AC-ST	AC-ZN
Alkanes	0.08	0.65			
Benzene		0.83	0.49		49.05
Toluene	5.58	4.9	8.23	0.52	10.62
Ethylbenzene	3.73	25.59	28.59	0.4	4.01
Styrene	65.51	43.51	39.11	0.36	4.87
.alpha.-Methyl Styrene	7.71	5.87	7.16		
Other Monocyclic Aromatics		0.35	2.16		
Naphthalene	0.57	9.29	5.36	0.46	2.83
Biphenyls	7.74	4.85	5.8	16.08	21.86
Other PAHs	0.19	4.16	2.86	2.41	2.5
Benzoic Acid				22.5	0.78
Acetophenone				15.17	1.51
Benzophenone				17.39	0.22
Others	0.5		0.24		

As shown in Table 4, catalytic pyrolysis of PET over AC-ST primarily yields benzoic acid, acetophenone, benzophenone, and biphenyls (accounting for 22.5%, 15.17%, 17.39%, and 16.08%, respectively). The benzoic acid and acetophenone are formed via decarboxylation of terephthalic acid and degradation of benzoic acid vinyl ester (P1, Scheme 1d) [41], respectively. Benzophenone is formed via the dehydration of benzoic acid and benzene. The biphenyl is formed via a combination of two benzene rings (P7, Scheme 1d) [42]. Toluene and ethylbenzene, with less than 1%, are also found in the liquid of AC-ST. Toluene and ethylbenzene might be derived from the alkylation of benzene. When the AC-ZN catalyzes the PET pyrolysis, and the deoxygenation of the oxygenated compounds takes place considerably [43], resulting in the content of monoaromatics increasing to more than

60%. However, the pyrolysis of PET on AC-HP does not yield liquid products for no apparent reason.

In the gas products of LDPE, PP, and PS, the C1-C3 alkanes, olefins, and hydrogen are the primary components (Figure 5). In addition to C1-C3 alkanes and olefins, 20% C_7H_{14} and 14% C_6H_{14} are found in the gas of LDPE and PP catalyzed by AC-ST. PET's gas products are mainly CO and CO_2 [44,45]. Significantly higher hydrogen contents are found in the gas of four plastic catalyzed by AC-HP and AC-ZN than AC-ST. The AC-ZN yields a highest percentage of H_2 in gas in three plastics due to the strong dehydrogenation capability of the Zn-involved species [46].

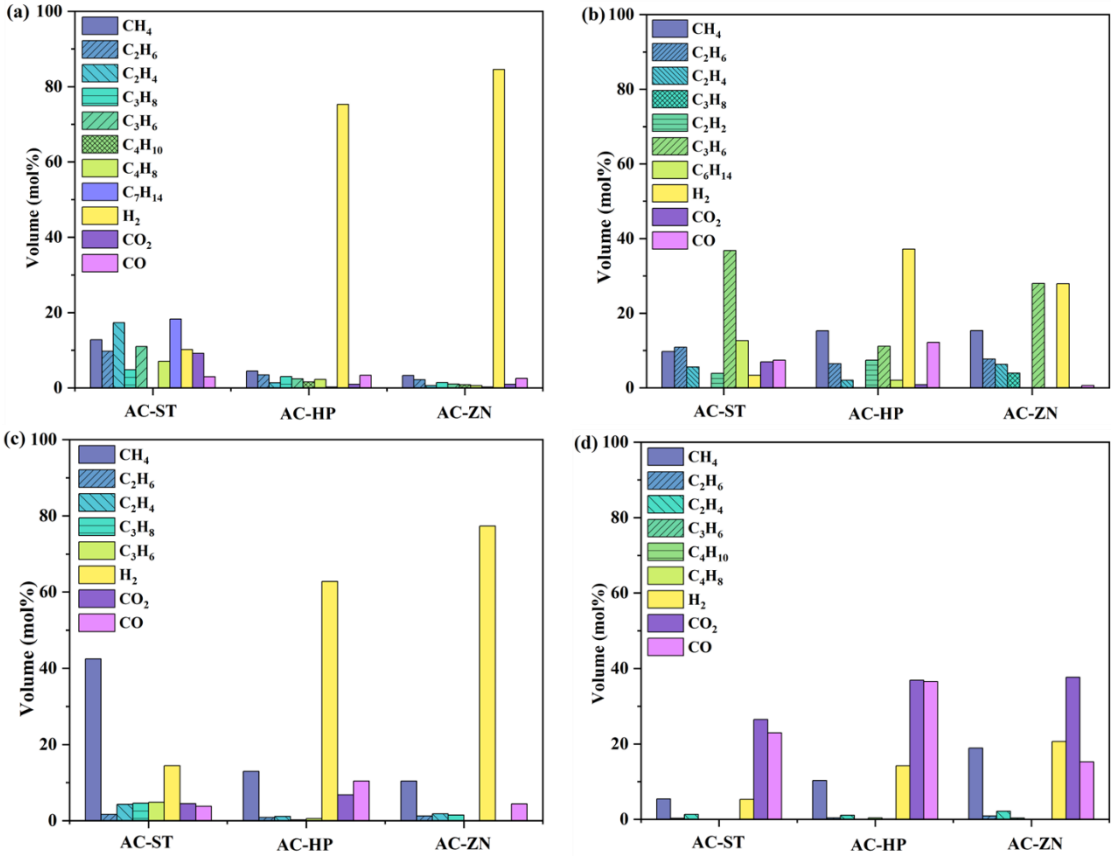

Figure 5. Components of the gas products are catalyzed by carbon modified by steam, H_3PO_4, and $ZnCl_2$. (**a**) LDPE, (**b**) PP, (**c**) PS, (**d**) PET.

3.4. Effects of Mass Ratio of Activator on Carbons' Performance

The effects of the mass ratio of phosphorous and zinc chloride to industrial organic solid waste are studied on the pyrolysis of LDPE. Tables S2 and S3 show LDPE's product yield and distributions under different activation conditions. The increased mass ratio of AC-HP results in a more profound degradation of LDPE. The AC-HP prepared at mass ratio 1:1 cannot effectively catalyze LDPE degradation, and the wax is the main product. When the mass ratio increases to 1.5, the LDPE is entirely decomposed into liquid and gaseous products. At the mass ratio of two, as much as 78.5 wt.% of gas was recovered.

$ZnCl_2$ seems more effective than H_3PO_4 in activating industrial organic solid waste for catalytic pyrolysis of LDPE. At the mass ratio of 0.5, only 22 wt.% of solid residue is received, much lower than that of AC-HP1. When the $ZnCl_2$ mass ratio increases to 1.5, the LDPE completely degrades into gas (89.50 wt.%) and liquid (10.5 wt.%). The variation in product yield with increasing $ZnCl_2$ mass ratio could be due to the different strength, concentration, and location of the Lewis and Bronsted acid site on the carbon [34]. These factors would change the reaction routes and kinetics during polymer degradation [47].

In terms of the liquid composition, with increased H_3PO_4 and $ZnCl_2$ mass ratios, a small change was found for the contents of straight alkanes in the liquid, while the cycloalkanes reduced. It is also found that the content of PAHs increases with H_3PO_4 and $ZnCl_2$ mass ratio. This is probably because the increased acid sites promote the dehydrogenation of cycloalkanes and the condensation of phenyl rings.

3.5. Discussion of Possible Reaction Mechanism over Carbons

The possible reaction pathways of different plastics over carbons are presented in Scheme 1. The literature has discussed the reaction pathway of LDPE over carbon catalysts, which is similar with the findings of this study. Polyolefin pyrolysis proceeds through random scission, end-chain scission, or carbocation mechanisms [47]. At 500 °C, the thermal pyrolysis LDPE and PP are mainly subject to random C-C bond breaking and end-chain scission to produce a product with a carbon number larger than 30. The Bronsted acid sites on carbons promote radical transfer and carbocation formation, yielding products with a carbon number less than 20. The incorporation of P and Zn creates additional active sites for plastic conversion. On AC-HP, the P–OH, C–O–PO_3, and C–PO_3 form a tri-coordinated carbenium ion or penta-coordinated carbonium ion [36], which is deprotonated to produce hydrogen or proceeds to C-C scission to produce olefins or alkanes.

Meanwhile, the light olefins may undergo oligomerization, cyclization, or Diels–Alder to form monoaromatics. Cooperation of P=O and C=O also occurs, enhancing the dehydrogenation capability. On AC-ZN, the zinc cation species or ZnO [48] play an essential role in aromatization (P7, P8, Scheme 1a). The olefins first oligomerize on the zinc species to produce a polyene-like hydrocarbon. Then, the generated polyene-like hydrocarbon was stabilized on zinc species with subsequent dehydrogenation to form highly unsaturated dienes or allenes. The highly unsaturated dienes or allenes are finally protonated by the nearby Bronsted acid site, followed by chain cyclization and deprotonation to produce monoaromatics.

The reaction pathways of PS and PET over carbon catalysts or solid acid catalysts are rarely reported. Based on our data, the pyrolysis of PS is inferred to involve thermal and catalytic degradation. Thermal degradation of PS undergoes random scission and end-chain scission to form an oligomer of styrenes [49]. During the catalytic degradation, the Bronsted acid sites protonated the carbon on the rings which transforms to a penta-coordinated carbocation [40]. The protonated carbocation on the ring then undergoes dealkylation (P2, Scheme 1c) to form benzene and phenyl cations. Meanwhile, the phenyl cations might undergo β-scission to form toluene, ethylbenzene, and styrene (P6, Scheme 1c). P- and Zn-involved acid sites extract hydride ions from the benzyl carbon, generating a tri-coordinated [38] carbocation, which undergoes β-scission and hydride transfer to yield benzene and ethylbenzene (P4 and P5, Scheme 1c).

The catalytic product of PET indicated that degradation of PET might begin with beta hydrogen transfer, followed by ester bond breakage to form carboxyl- and vinyl-terminated products (P1, Scheme 1d) [50,51]. The vinyl ester groups on the vinyl benzoate are then rearranged and decarbonylated to form acetophenone (P2, Scheme 1d). The dehydration of benzoic acid and benzene coupling may occur to form benzophenone (P5, Scheme 1d). In the presence of AC-ZN, successive decarboxylation of terephthalic acid takes place to produce CO_2 and benzene (P3, P4, Scheme 1d). The benzene undergoes a reaction of alkylation to form toluene or ring combination to form biphenyl and polycyclic aromatic hydrocarbons (P6 and P7, Scheme 1d).

4. Conclusions

The catalytic pyrolysis of waste plastics over industrial organic solid-waste-derived carbon was investigated. The effects of the activation method on the carbon's catalytic performance are discussed. The thermogravimetric results indicate that all three carbons reduce the temperature of plastic pyrolysis. Chemical activation using H_3PO_4 and $ZnCl_2$ produces carbon with a higher specific surface area and more abundant porosity than

steam/carbon. In addition, the H_3PO_4 and $ZnCl_2$ activation create P and Zn-involved acid sites on carbon. These characteristics of AC-HP and AC-ZN contribute to their better catalytic performance in degrading plastics than AC-ST. The AC-HP and AC-ZN promote: (1) C-C cracking and aromatization of polyolefins; (2) the protonation of phenyl carbon of PS to yield higher benzene, toluene, and ethylbenzene; and (3) the decarboxylation of the terephthalic acid intermediate of PET, resulting in higher CO_2 and benzene.

Supplementary Materials: The following supporting information can be downloaded at: https://www.mdpi.com/article/10.3390/pr10122668/s1, Figure S1. The N_2 adsorption/desorption isotherms (a) and pore size distribution (b) of AC-ST, AC-HP, and AC-ZN; Figure S2. Carbon distributions of products for upgrading of LDPE using activated carbon; Figure S3. Carbon distributions of liquid products for upgrading of PP using activated carbon; Figure S4. Carbon distributions of liquid products for upgrading of PS using activated carbon; Figure S5. Carbon number distributions of liquid products for upgrading of PET using activated carbon; Table S1. Pyrolysis characteristics of plastics and activated carbon mixture at a heating rate of 10 °C/min; Table S2. Product yields under different activation conditions; Table S3. Components of the oil products on LDPE catalyzed by activated carbon modified by H_3PO_4, and $ZnCl_2$ under different activation conditions.

Author Contributions: Conceptualization, K.Q.; methodology, K.Q.; experimental data curation, W.T., W.L. and S.W.; writing—original draft preparation, K.Q. and W.T.; writing—review and editing, K.Q. and Y.F.; visualization, W.T.; supervision, D.C.; funding acquisition, K.Q. All authors have read and agreed to the published version of the manuscript.

Funding: This research was funded by The National Higher-education Institution General Research and Development Project grant number [22120210538], National Natural Science Foundation of China grant number [52106266].

Data Availability Statement: The data will be available when requested.

Conflicts of Interest: The authors declare no conflict of interest.

References

1. Jehanno, C.; Alty, J.W.; Roosen, M.; De Meester, S.; Dove, A.P.; Chen, E.Y.-X.; Leibfarth, F.A.; Sardon, H. Critical Advances and Future Opportunities in Upcycling Commodity Polymers. *Nature* **2022**, *603*, 803–814. [CrossRef]
2. Rosenboom, J.-G.; Langer, R.; Traverso, G. Bioplastics for a Circular Economy. *Nat. Rev. Mater.* **2022**, *7*, 117–137. [CrossRef] [PubMed]
3. Geyer, R.; Jambeck, J.R.; Law, K.L. Production, Use, and Fate of All Plastics Ever Made. *Sci. Adv.* **2017**, *3*, e1700782. [CrossRef]
4. Liu, Y.; Guo, D.; Dong, L.; Xu, Y.; Liu, J. Pollution Status and Environmental Sound Management (ESM) Trends on Typical General Industrial Solid Waste. *Procedia Environ. Sci.* **2016**, *31*, 615–620. [CrossRef]
5. Yang, Z.; Chen, H.; Du, L.; Lu, W.; Qi, K. Exploring the Industrial Solid Wastes Management System: Empirical Analysis of Forecasting and Safeguard Mechanisms. *J. Environ. Manag.* **2021**, *279*, 111627. [CrossRef] [PubMed]
6. Zhou, B.; Sun, C.; Yi, H. Solid Waste Disposal in Chinese Cities: An Evaluation of Local Performance. *Sustainability* **2017**, *9*, 2234. [CrossRef]
7. Wu, L.; Jiang, X.; Lv, G.; Li, X.; Yan, J. Interactive Effect of the Sorted Components of Solid Recovered Fuel Manufactured from Municipal Solid Waste by Thermogravimetric and Kinetic Analysis. *Waste Manag.* **2020**, *102*, 270–280. [CrossRef]
8. Parthasarathy, P.; Sheeba, K.N. Generation of Fuel Char through Biomass Slow Pyrolysis. *Energy Sources Part Recovery Util. Environ. Eff.* **2017**, *39*, 599–605. [CrossRef]
9. Arribas, L.; Arconada, N.; González-Fernández, C.; Löhrl, C.; González-Aguilar, J.; Kaltschmitt, M.; Romero, M. Solar-Driven Pyrolysis and Gasification of Low-Grade Carbonaceous Materials. *Int. J. Hydrogen Energy* **2017**, *42*, 13598–13606. [CrossRef]
10. Parthasarathy, P.; Al-Ansari, T.; Mackey, H.R.; Sheeba Narayanan, K.; McKay, G. A Review on Prominent Animal and Municipal Wastes as Potential Feedstocks for Solar Pyrolysis for Biochar Production. *Fuel* **2022**, *316*, 123378. [CrossRef]
11. Zhang, Y.; Duan, D.; Lei, H.; Villota, E.; Ruan, R. Jet Fuel Production from Waste Plastics via Catalytic Pyrolysis with Activated Carbons. *Appl. Energy* **2019**, *251*, 113337. [CrossRef]
12. Sun, K.; Huang, Q.; Ali, M.; Chi, Y.; Yan, J. Producing Aromatic-Enriched Oil from Mixed Plastics Using Activated Biochar as Catalyst. *Energy Fuels* **2018**, *32*, 5471–5479. [CrossRef]
13. Mei, Z.; He, X.; Chen, D.; Wang, N.; Yin, L.; Qian, K.; Feng, Y. Comparison of Chars from Municipal Solid Waste and Wheat Straw for Understanding the Role of Inorganics in Char-Based Catalysts during Volatile Reforming Process. *Energy* **2021**, *229*, 120619. [CrossRef]
14. Mei, Z.; Chen, D.; Qian, K.; Zhang, R.; Yu, W. Producing Eco-Methane with Raw Syngas Containing Miscellaneous Gases and Tar by Using a Municipal Solid Waste Char-Based Catalyst. *Energy* **2022**, *254*, 124244. [CrossRef]

15. Tsyntsarski, B.; Stoycheva, I.; Tsoncheva, T.; Genova, I.; Dimitrov, M.; Petrova, B.; Paneva, D.; Cherkezova-Zheleva, Z.; Budinova, T.; Kolev, H.; et al. Activated Carbons from Waste Biomass and Low Rank Coals as Catalyst Supports for Hydrogen Production by Methanol Decomposition. *Fuel Process. Technol.* **2015**, *137*, 139–147. [CrossRef]
16. Fu, G.; Wang, Z.; Zhang, Y.; Huang, Z.; Liu, J.; Zhou, J.; Cen, K. Effect of Raw Material Sources on Activated Carbon Catalytic Activity for HI Decomposition in the Sulfur-Iodine Thermochemical Cycle for Hydrogen Production. *Int. J. Hydrogen Energy* **2016**, *41*, 7854–7860. [CrossRef]
17. Yeganeh, M.M.; Kaghazchi, T.; Soleimani, M. Effect of Raw Materials on Properties of Activated Carbons. *Chem. Eng. Technol.* **2006**, *29*, 1247–1251. [CrossRef]
18. Wani Likun, P.K.; Zhang, H. Insights into Pyrolysis of Torrefied-Biomass, Plastics/Tire and Blends: Thermochemical Behaviors, Kinetics and Evolved Gas Analyses. *Biomass Bioenergy* **2020**, *143*, 105852. [CrossRef]
19. Sun, K.; Huang, Q.; Meng, X.; Chi, Y.; Yan, J. Catalytic Pyrolysis of Waste Polyethylene into Aromatics by H_3PO_4-Activated Carbon. *Energy Fuels* **2018**, *32*, 9772–9781. [CrossRef]
20. Ţucureanu, V.; Matei, A.; Avram, A.M. FTIR Spectroscopy for Carbon Family Study. *Crit. Rev. Anal. Chem.* **2016**, *46*, 502–520. [CrossRef]
21. Yudianti, R.; Onggo, H.; Sudirman; Saito, Y.; Azuma, J.I. Analysis of Functional Group Sited on Multi-Wall Carbon Nanotube Surface. *Open Mater. Sci. J.* **2011**, *5*, 242–247. [CrossRef]
22. Obreja, A.C.; Cristea, D.; Gavrila, R.; Schiopu, V.; Dinescu, A.; Danila, M.; Comanescu, F. Isocyanate Functionalized Graphene/P3HT Based Nanocomposites. *Appl. Surf. Sci.* **2013**, *276*, 458–467. [CrossRef]
23. Hussain, Z.; Kumar, R. Synthesis and Characterization of Novel Corncob-Based Solid Acid Catalyst for Biodiesel Production. *Ind. Eng. Chem. Res.* **2018**, *57*, 11645–11657. [CrossRef]
24. Hita, I.; Cordero-Lanzac, T.; Gallardo, A.; Arandes, J.M.; Rodríguez-Mirasol, J.; Bilbao, J.; Cordero, T.; Castaño, P. Phosphorus-Containing Activated Carbon as Acid Support in a Bifunctional Pt–Pd Catalyst for Tire Oil Hydrocracking. *Catal. Commun.* **2016**, *78*, 48–51. [CrossRef]
25. Qiu, T.; Yang, J.-G.; Bai, X.-J.; Wang, Y.-L. The Preparation of Synthetic Graphite Materials with Hierarchical Pores from Lignite by One-Step Impregnation and Their Characterization as Dye Absorbents. *RSC Adv.* **2019**, *9*, 12737–12746. [CrossRef]
26. Westerhout, R.W.J.; Waanders, J.; Kuipers, J.A.M.; van Swaaij, W.P.M. Kinetics of the Low-Temperature Pyrolysis of Polyethene, Polypropene, and Polystyrene Modeling, Experimental Determination, and Comparison with Literature Models and Data. *Ind. Eng. Chem. Res.* **1997**, *36*, 1955–1964. [CrossRef]
27. Williams, P.T.; Williams, E.A. Interaction of Plastics in Mixed-Plastics Pyrolysis. *Energy Fuels* **1999**, *13*, 188–196. [CrossRef]
28. Al-Salem, S.M.; Antelava, A.; Constantinou, A.; Manos, G.; Dutta, A. A Review on Thermal and Catalytic Pyrolysis of Plastic Solid Waste (PSW). *J. Environ. Manag.* **2017**, *197*, 177–198. [CrossRef]
29. Zhao, D.; Wang, X.; Miller, J.B.; Huber, G.W. The Chemistry and Kinetics of Polyethylene Pyrolysis: A Process to Produce Fuels and Chemicals. *ChemSusChem* **2020**, *13*, 1764–1774. [CrossRef] [PubMed]
30. Escande, V.; Olszewski, T.K.; Grison, C. Preparation of Ecological Catalysts Derived from Zn Hyperaccumulating Plants and Their Catalytic Activity in Diels–Alder Reaction. *C. R. Chim.* **2014**, *17*, 731–737. [CrossRef]
31. Fanchiang, W.-L.; Lin, Y.-C. Catalytic Fast Pyrolysis of Furfural over H-ZSM-5 and Zn/H-ZSM-5 Catalysts. *Appl. Catal. Gen.* **2012**, *419–420*, 102–110. [CrossRef]
32. Li, L.; Zhu, W.; Liu, Y.; Shi, L.; Liu, H.; Ni, Y.; Liu, S.; Zhou, H.; Liu, Z. Phosphorous-Modified Ordered Mesoporous Carbon for Catalytic Dehydrogenation of Propane to Propylene. *RSC Adv.* **2015**, *5*, 56304–56310. [CrossRef]
33. Kruse, T.M.; Wong, H.-W.; Broadbelt, L.J. Mechanistic Modeling of Polymer Pyrolysis: Polypropylene. *Macromolecules* **2003**, *36*, 9594–9607. [CrossRef]
34. Lashchinskaya, Z.N.; Gabrienko, A.A.; Arzumanov, S.S.; Kolganov, A.A.; Toktarev, A.V.; Freude, D.; Haase, J.; Stepanov, A.G. Which Species, Zn^{2+} Cations or ZnO Clusters, Are More Efficient for Olefin Aromatization? 13C Solid-State NMR Investigation of n-But-1-Ene Transformation on Zn-Modified Zeolite. *ACS Catal.* **2020**, *10*, 14224–14233. [CrossRef]
35. Huang, J.; Li, X.; Meng, H.; Tong, H.; Cai, X.; Liu, J. Studies on Pyrolysis Mechanisms of Syndiotactic Polystyrene Using DFT Method. *Chem. Phys. Lett.* **2020**, *747*, 137334. [CrossRef]
36. Verma, A.; Sharma, S.; Pramanik, H. Pyrolysis of Waste Expanded Polystyrene and Reduction of Styrene via In-Situ Multiphase Pyrolysis of Product Oil for the Production of Fuel Range Hydrocarbons. *Waste Manag.* **2021**, *120*, 330–339. [CrossRef] [PubMed]
37. Adnan; Shah, J.; Jan, M.R. Polystyrene Degradation Studies Using Cu Supported Catalysts. *J. Anal. Appl. Pyrolysis* **2014**, *109*, 196–204. [CrossRef]
38. Karmore, V.; Madras, G. Thermal Degradation of Polystyrene by Lewis Acids in Solution. *Ind. Eng. Chem. Res.* **2002**, *41*, 657–660. [CrossRef]
39. Lee, S.-Y.; Yoon, J.-H.; Kim, J.-R.; Park, D.-W. Degradation of Polystyrene Using Clinoptilolite Catalysts. *J. Anal. Appl. Pyrolysis* **2002**, *64*, 71–83. [CrossRef]
40. Marczewski, M.; Kamińska, E.; Marczewska, H.; Godek, M.; Rokicki, G.; Sokołowski, J. Catalytic Decomposition of Polystyrene. The Role of Acid and Basic Active Centers. *Appl. Catal. B Environ.* **2013**, *129*, 236–246. [CrossRef]
41. Du, S.; Valla, J.A.; Parnas, R.S.; Bollas, G.M. Conversion of Polyethylene Terephthalate Based Waste Carpet to Benzene-Rich Oils through Thermal, Catalytic, and Catalytic Steam Pyrolysis. *ACS Sustain. Chem. Eng.* **2016**, *4*, 2852–2860. [CrossRef]

42. Dhahak, A.; Hild, G.; Rouaud, M.; Mauviel, G.; Burkle-Vitzthum, V. Slow Pyrolysis of Polyethylene Terephthalate: Online Monitoring of Gas Production and Quantitative Analysis of Waxy Products. *J. Anal. Appl. Pyrolysis* **2019**, *142*, 104664. [CrossRef]
43. Kumagai, S.; Yamasaki, R.; Kameda, T.; Saito, Y.; Watanabe, A.; Watanabe, C.; Teramae, N.; Yoshioka, T. Tandem μ-Reactor-GC/MS for Online Monitoring of Aromatic Hydrocarbon Production via CaO-Catalysed PET Pyrolysis. *React. Chem. Eng.* **2017**, *2*, 776–784. [CrossRef]
44. Artetxe, M.; Lopez, G.; Amutio, M.; Elordi, G.; Olazar, M.; Bilbao, J. Operating Conditions for the Pyrolysis of Poly-(Ethylene Terephthalate) in a Conical Spouted-Bed Reactor. *Ind. Eng. Chem. Res.* **2010**, *49*, 2064–2069. [CrossRef]
45. Veksha, A.; Ahamed, A.; Wu, X.Y.; Liang, L.; Chan, W.P.; Giannis, A.; Lisak, G. Technical and Environmental Assessment of Laboratory Scale Approach for Sustainable Management of Marine Plastic Litter. *J. Hazard. Mater.* **2022**, *421*, 126717. [CrossRef]
46. Savage, P.E. Mechanisms and Kinetics Models for Hydrocarbon Pyrolysis. *J. Anal. Appl. Pyrolysis* **2000**, *54*, 109–126. [CrossRef]
47. Vollmer, I.; Jenks, M.J.F.; Roelands, M.C.P.; White, R.J.; van Harmelen, T.; de Wild, P.; van der Laan, G.P.; Meirer, F.; Keurentjes, J.T.F.; Weckhuysen, B.M. Beyond Mechanical Recycling: Giving New Life to Plastic Waste. *Angew. Chem. Int. Ed.* **2020**, *59*, 15402–15423. [CrossRef]
48. Kazansky, V.B.; Serykh, A.I.; Pidko, E.A. DRIFT Study of Molecular and Dissociative Adsorption of Light Paraffins by HZSM-5 Zeolite Modified with Zinc Ions: Methane Adsorption. *J. Catal.* **2004**, *225*, 369–373. [CrossRef]
49. Park, K.-B.; Jeong, Y.-S.; Guzelciftci, B.; Kim, J.-S. Two-Stage Pyrolysis of Polystyrene: Pyrolysis Oil as a Source of Fuels or Benzene, Toluene, Ethylbenzene, and Xylenes. *Appl. Energy* **2020**, *259*, 114240. [CrossRef]
50. Buxbaum, L.H. The Degradation of Poly(Ethylene Terephthalate). *Angew. Chem. Int. Ed.* **1968**, *7*, 182–190. [CrossRef]
51. McNeill, I.C.; Bounekhel, M. Thermal Degradation Studies of Terephthalate Polyesters: 1. Poly(Alkylene Terephthalates). *Polym. Stabilisation Mech. Appl.* **1991**, *34*, 187–204. [CrossRef]